Journal of Geochemical Exploration 269 (2025) 107635

Contents lists available at ScienceDirect

Journal of Geochemical Exploration

journal homepage: www.elsevier.com/locate/gexplo

Mapping geochemical anomalies using angle-based outlier detection approach

Shahed Shahrestani *, Ioan Sanislav

College of Science and Engineering, Economic Geology Research Centre (EGRU), James Cook University, Townsville, Australia

ARTICLE INFO

Keywords:
Outlier detection
ABOD
FastABOD
ICA
Geochemical anomaly
Mineral occurrence

ABSTRACT

This study evaluates the effectiveness of the angle-based outlier detection (ABOD) method in identifying geochemical anomalies in the Ahar-Arasbaran Zone (AAZ) within the Alborz-Azerbaijan Magmatic Belt (AAMB), known for its diverse mineralization such as Cu-Mo porphyry deposits, epithermal base and precious metal veins, and Fe-Cu skarn deposits. ABOD and its fast approximation (FastABOD) were applied to datasets with 9 (Selective) and 32 (All) features. Results showed that with fewer variables, the performance difference between ABOD and FastABOD decreased, highlighting the impact of dimensionality on anomaly detection. Geochemical anomaly maps (ABOD_All, ABOD_Selective, FastABOD_All, FastABOD_Selective) were assessed for detecting known mineralization. ABOD_Selective demonstrated superior performance, effectively placing 76 % of skarn and 70 % of porphyry mineral occurrences into the highest anomaly class, despite its overall performance being approximately 61 %.

Additionally, ABOD was compared with independent component analysis (ICA), focusing on IC2 and IC5. ICA effectively highlighted unique geochemical patterns, with IC2 excelling in identifying Cu-enriched zones and ABOD effectively delineating both Au- and Cu-bearing zones. ABOD was also compared with local outlier detection methods LOF, kNN, and iNNE. LOF showed distinct anomaly distributions due to its local density approach, while kNN, iNNE, and FastABOD produced similar maps based on distance, isolation, and angle-distance. ROC analysis revealed no significant performance difference, though FastABOD showed slight superiority, particularly with mineralized samples as validation points. Moreover, applying principal component analysis (PCA) as feature selection method enhanced the performance of the FastABOD method in delineating geochemical anomalies related to hydrothermal mineralization. Finally, random forest regression identified key elements such as Sb, Au, As, and Cu as significant in distinguishing geochemical signals from various mineralization types.

1. Introduction

Geochemical exploration often involves analyzing datasets with numerous variables, making multivariable outlier detection methods crucial for identifying anomalous patterns that may indicate mineral deposits (e.g., Shahrestani et al., 2020). Outliers in geochemical data can represent rare but significant geological features, providing valuable insights for mineral prospectivity mapping (e.g., Chen et al., 2023; Wang and Zuo, 2022; Shahrestani et al., 2020). An outlier is a data point that significantly deviates from the typical pattern of the dataset. It does not conform to the expected behavior of other points, making it an anomaly (e.g., Hodge and Austin, 2004). The challenge of detecting outliers has been approached through diverse methods, typically categorized into global and local models. Global models classify an object simply as an outlier or not, offering a binary outcome. On the other hand, local models compare data points to their neighbors within a localized region of the dataset, providing a more nuanced measure called an "outlier factor," which rates each object based on its deviation from expected norms. In applications where ranking the outliers in a database and retrieving the top-n outliers is important, a local outlier approach is clearly preferable (Kriegel et al., 2008). Based on the features that are utilized, outlier identification methods can be classified into several categories: statistical-based, distance-based, density-based, clustering-based, graph-based, ensemble-based, and learning-based approaches (Wang et al., 2019). For example, the core idea behind density-based outlier detection methods is that outliers are typically found in sparse

* Corresponding author.
E-mail address: shahrestanishahed1987@gmail.com (S. Shahrestani).

https://doi.org/10.1016/j.gexplo.2024.107635
Received 24 May 2024; Received in revised form 3 November 2024; Accepted 13 November 2024
Available online 19 November 2024

or low-density regions of the dataset, whereas inliers are situated in densely populated areas (Breunig et al., 2000).

In the fields of geochemical anomaly detection and mineral prospectivity mapping, a range of outlier detection methods has been applied. These methods encompass one-class support vector machines (OCSVMs) (Chen and Wu, 2017), isolation forest (iForest) (Chen and Wu, 2019), and bat-optimized OCSVM (Chen et al., 2019), distance anomaly factors (Chen et al., 2021a), k-nearest neighbor (Chen et al., 2021b,c), DBSCAN (Hajihosseinlou et al., 2024a), OPTICS (Hajihosseinlou et al., 2024b), and local outlier factor (LOF) (e.g., Shahrestani and Carranza, 2024; Puchhammer et al., 2024), deep autoencoder networks (e.g., Esmaeiloghli et al., 2023) among others. For instance, Chen et al. (2021c) concluded that the average method, maximization method, average of maximum (AOM) method, and maximum of average (MOA) method effectively enhance the robustness of k-nearest neighbor (kNN)-based anomaly detectors for high-dimensional geochemical data. The average method provides consistent performance, the maximization method excels in detecting significant anomalies, AOM balances these strengths, and MOA prioritizes models with consistently higher scores. These ensemble approaches outperform individual models including kNN, Gaussian mixture model (GMM), OCSVM, and iForest, making them reliable tools for complex geochemical anomaly detection. In another study, Shahrestani and Carranza (2024) compared the effectiveness of OCSVM, LOF, and iForest in delineating geochemical anomalies derived from different mineral deposit types. The study revealed that the selection of different outlier detection methods yields different geochemical anomaly patterns. For instance, OCSVM was trained only based on normal data set and demonstrated superiority in capturing Au and Cu mineralization. Moreover, Puchhammer et al. (2024) applied LOF, REG (regularized spatial detection technique), ROB (robust local outlier detection method), and ssMRCD (spatially smoothed minimum regularized covariance determinant) methods in geochemical anomaly detection for mineral exploration. They concluded that each local outlier detection method has distinct strengths and limitations in the context of mineral exploration. The LOF method effectively identifies isolated outliers but may miss anomalies in densely sampled areas with gradual changes, such as mineralized zones. The REG and ROB methods can produce different sets of outliers due to their internal workings and may struggle in regions with significant geochemical variability. The ssMRCD method is preferred for its ability to smoothly handle changes in covariance across neighborhoods, making it more reliable for detecting mineralization-related anomalies.

All outlier detection methods face various degrees of limitations. Firstly, techniques like k-nearest neighbor, local outlier factor, one-class support vector machines, and iforest struggle with the curse of dimensionality, especially in high-dimensional data, constraining their applicability to lower-dimensional datasets. The ‘curse of dimensionality’ (Bellman, 1966) refers to the exponential increase in complexity and computational challenges as the number of dimensions or features in a dataset grows. Consequently, as dimensionality increases, the relative difference between the farthest and closest distances diminishes, reducing the effectiveness of distance-based measures. Secondly, many approaches require the selection and tuning of hyperparameters, such as determining the number of clusters for clustering-based models, the architecture of layers for neural network-based models, and the choices of individual classifiers for ensemble models. However, this process can be subjective and yield diverse results (e.g., Alimohammadi and Chen, 2022; Li et al., 2020). Despite these challenges, the main rationale for utilizing angle-based anomaly detection is the acknowledgment that in high-dimensional spaces, conventional concepts like distance, proximity, and nearest neighbor lose their relevance as the number of dimensions rises (Aggarwal et al., 2001). This paper presents the utilization of angle-based outlier detection, a local outlier detection method, in a geochemical multivariate dataset to identify anomalies. The method calculates the variance in angles between a sample point and all pairs of other points, providing a novel approach for anomaly detection in high-dimensional geochemical data. The identified anomalies are then compared with those obtained through independent component analysis (ICA). The study evaluates the effectiveness of these geochemical anomalies in delineating mineralized zones, highlighting the potential of angle-based outlier detection as a valuable tool in geochemical exploration and mineral prospectivity mapping.

2. Materials and methods

2.1. Case study

The Alborz Magmatic Belt (AMB) in NW Iran is part of the Tethyan Eurasian Metallogenic Belt, situated along the western and southern coast of the Caspian Sea, bounded by the Eurasian Plate to the north and the Arabian Plate to the south. Arc-related magmatism in the AMB initiated in the Upper Jurassic and persisted intermittently until the Quaternary (Alavi, 1991; Dilek et al., 2010; Shamanian and Hattori, 2021). The western section of the AMB merges with the Urumieh-Dokhtar Magmatic Belt (UDMB), termed as the Alborz-Azerbaijan Magmatic Belt (AAMB). Within the AAMB lies the Ahar-Arasbaran Zone (AAZ), hosting Cenozoic igneous rocks such as granodiorite, tonalite, monzonite, and quartz monzonite, featuring a typical arc signature (Aghaei et al., 2023; Ghorbani, 2013). Magmatic events in the AAZ began during the Late Cretaceous–Paleocene period and continued with shoshonitic magmatism in the Late Eocene–Oligocene epoch, with significant mineralization occurring in the Late Oligocene and Early Miocene (Jamali et al., 2010).

The AAZ hosts diverse mineral deposits, including Cu-Mo porphyry deposits, epithermal base and precious metal veins, porphyry-related Cu-Mo-Au vein type deposits, intrusion-related gold deposits, and Fe-Cu skarn deposits. Porphyry Cu deposits tend to form predominantly in island and continental-arc settings like the UDMB. Exploration studies and known mineral occurrences in the northern parts of the UDMB, especially in the Varzaghan district, suggest considerable potential for porphyry Cu deposits in Iran. The Varzaghan district, situated in the northern part of the AAZ, comprises primarily I-type granitoids and monzonites formed due to intense magmatic activity during the Eocene that continued into the Oligocene–Miocene with the emplacement of large intrusions that caused extensive alteration and locally economic mineralization (e.g., Aghaei et al., 2023; Kouhestani et al., 2018; Ghezelbash and Maghsoudi, 2018; Aghazadeh et al., 2015; Cooke et al., 2005).

The key lithologies in the study area include Cretaceous sedimentary and volcanic units, located mainly in the northern Varzaghan district, and Eocene–Oligocene volcanics like trachyandesite, andesitic basalt, and porphyritic andesite (Fig. 1). Oligo-Miocene granodiorites to quartz-monzonites intrude these formations. Plio-Quaternary andesitic and basaltic rocks overlay the older magmatic units, primarily in the southern region, whereas Quaternary alluvial deposits comprising gravel, sand, and silty clay are widespread in river plains. The mineralization in the region is associated with intense hydrothermal alteration linked to Oligo-Miocene intrusive rocks of calc-alkaline to alkaline compositions (Jamali et al., 2010; Mehrpartou, 1993).

In the northern parts of Arasbaran, particularly in the Varzaghan district, porphyry deposits exhibit geochemical signatures linked to Cu, Au, Mo, and Bi mineralization (Jamali et al., 2010; Maghsoudi et al., 2014). Notably, significant Cu skarn deposits surround the Oligocene–Miocene Ahar batholith, believed to have led to contact metamorphism, contact metasomatic mineralization, and skarn formation. Cu skarn deposits in this zone are associated with I-type calc-alkaline plutons with porphyritic textures displaying contact metamorphism with an intrusive stock (Meinert, 1992; Moazzen and Modjarrad, 2005; Mollai et al., 2009). Further details on various skarn mineralization occurrences in the study area can be explored in Mollai et al. (2009); Parsa et al. (2017), and Hassanpour (2013).

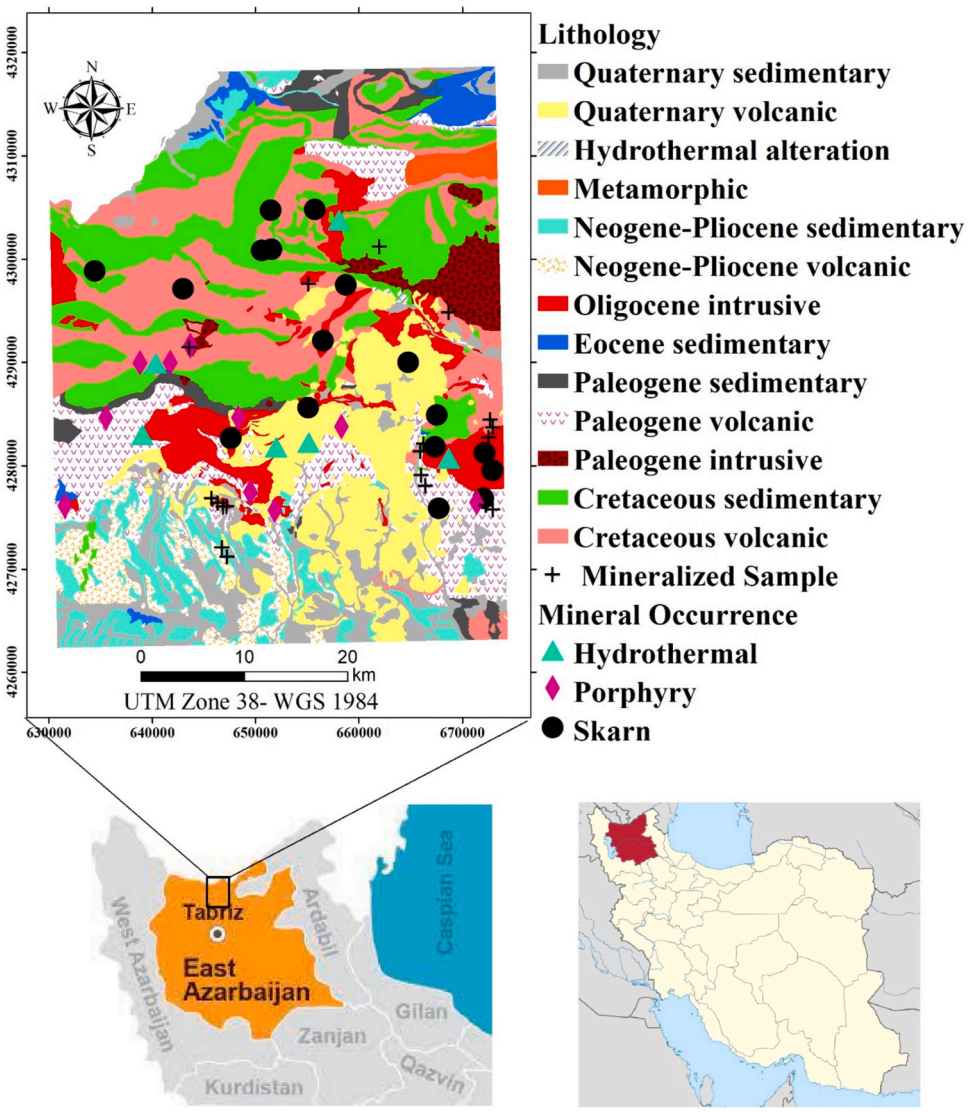

Fig. 1. Simplified geological map of the study area based on Mehrpartou (1993).

2.2. Geochemical data

In 2007, the geological survey of Iran conducted a comprehensive stream sediment survey in the Varzaghan area, collecting a total of 1067 sediment samples with the sampling density of 0.45 sample per km^2 (Fig. 2). Each sample, weighing between 200 and 300 g, consisted primarily of the <80 μm fraction. Subsequently, the chemical composition of these samples was analyzed at Alborz Zarkavan Company by ICP-OES. Additionally, the samples were subjected to specific analysis for Au content using the Fire-Assay technique. The detection limits for trace elements were at 0.01 ppm, except for As (0.1 ppm), Bi (0.2 ppm), Sb (0.5 ppm), and Zn (50 ppm). The precision of the laboratory analysis was assessed by examining the results of 30 pulp duplicate samples using the quality control method outlined by Thompson and Howarth (1976). The laboratory precision was better than 10 % for all elements included in the analysis (Shahrestani et al., 2018).

2.3. Angle-based outlier detection (ABOD)

Angle-based outlier detection (ABOD) combines the analysis of distances and the directions of distance vectors to discern outliers from typical data points (Kriegel et al., 2008). By examining the angular differences between sets of distance vectors, i.e., the relative distances from the point to its neighbors, this method effectively distinguishes standard observations from anomalies, maintaining its utility across varying dimensional spaces. To illustrate the principles of the ABOD method, a two-dimensional case including Cu and Mo values of 100 samples were randomly chosen from the geochemical dataset of the study area. Triangles were formed by groups of three samples, and the angles between the vectors forming the triangle sides were computed. Within each cluster of points, the angles between different vectors showed a wide range of variation (Fig. 3). However, the histogram of angles revealed that for samples located on the periphery of a cluster, the variability in angles was noticeably reduced. In other words, a point is considered to be within a cluster if the spectrum of angles observed around it is wide, indicating that the point is surrounded by other points in various directions. In contrast, a point is likely positioned outside a cluster if the spectrum of observed angles around it is small, indicating that other points are located predominantly in specific directions.

The angle-based outlier factor (ABOF) for an object in the database T is calculated by computing the dot product of the difference vectors for each triplet of points. For any given query point $\vec{A}$ in T, all pairs ($\vec{B}$, $\vec{C}$) from the remaining points in T, excluding $\vec{A}$, are considered. This computed dot product is then normalized by the product of the lengths of the difference vectors. By using this normalization scheme, the influence of angles between vectors that point from the query point is

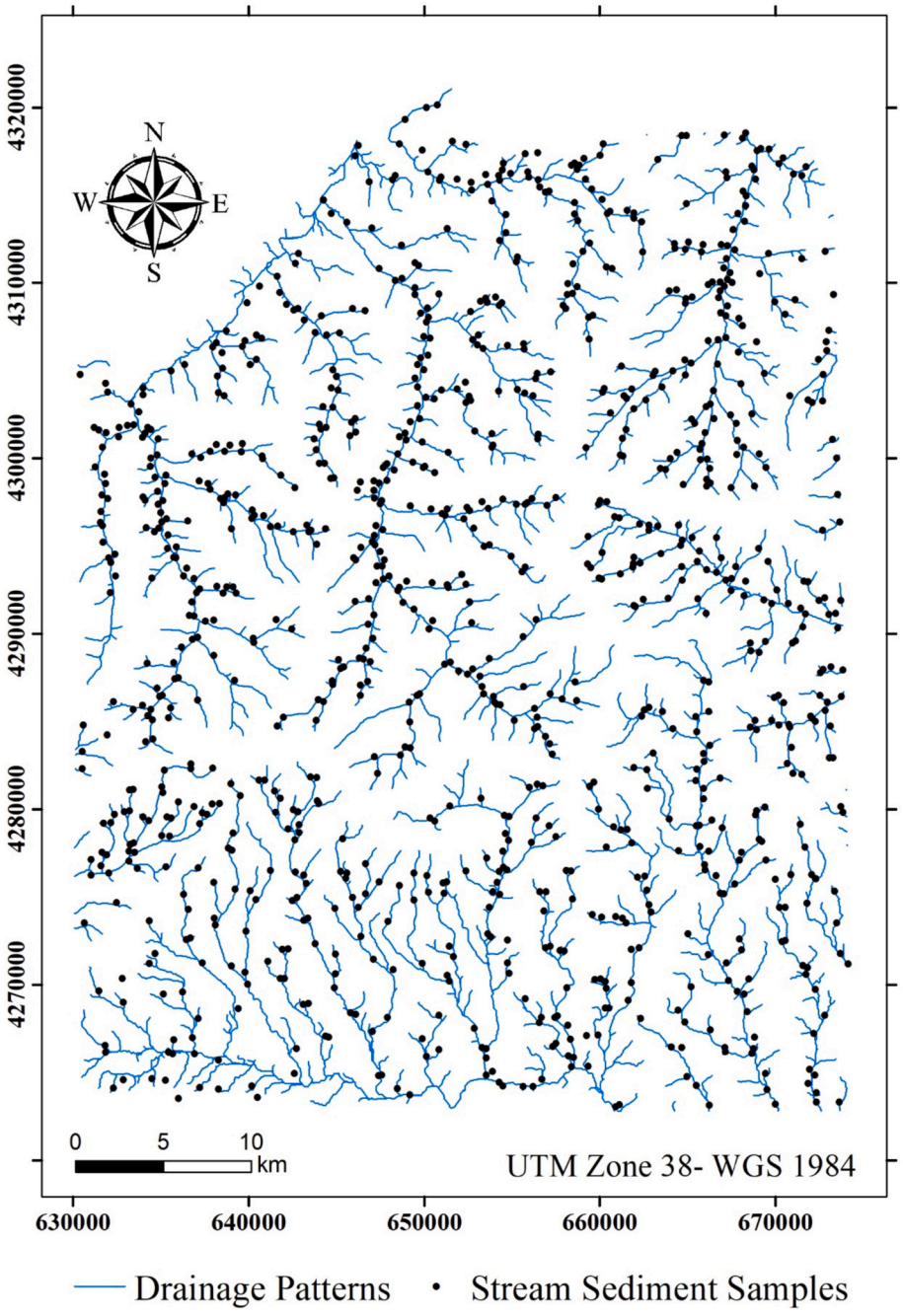

Fig. 2. Locations of stream sediment samples and associated rivers.

reduced if the corresponding points are far from the query point. Through this weighting factor, the impact of distance on the value is considered, albeit to a lesser extent. However, this weighting of the variance is crucial because naturally, the angle between a pair of points varies more significantly with a greater distance (Kriegel et al., 2008). The variation in this value across all pairs of points relative to the query point $\vec{A}$ defines the ABOF of $\vec{A}$:

$$ABOF_{\vec{A}} = Var_{\vec{B},\vec{C}\in T}\left(\frac{\langle \overline{AB}, \overline{AC}\rangle}{\|\overline{AB}\|^2 \cdot \|\overline{AC}\|^2}\right)$$

$$= \frac{\sum_{\vec{B}\in T}\sum_{\vec{C}\in T}\frac{1}{\|\overline{AB}\|\cdot\|\overline{AC}\|}\cdot\left(\frac{\langle \overline{AB}, \overline{AC}\rangle}{\|\overline{AB}\|^2 \cdot \|\overline{AC}\|^2}\right)^2}{\sum_{\vec{B}\in T}\sum_{\vec{C}\in T}\frac{1}{\|\overline{AB}\|\cdot\|\overline{AC}\|}} - \left(\frac{\sum_{\vec{B}\in T}\sum_{\vec{C}\in T}\frac{1}{\|\overline{AB}\|\cdot\|\overline{AC}\|}\cdot\left(\frac{\langle \overline{AB}, \overline{AC}\rangle}{\|\overline{AB}\|^2 \cdot \|\overline{AC}\|^2}\right)^2}{\sum_{\vec{B}\in T}\sum_{\vec{C}\in T}\frac{1}{\|\overline{AB}\|\cdot\|\overline{AC}\|}}\right) \quad (1)$$

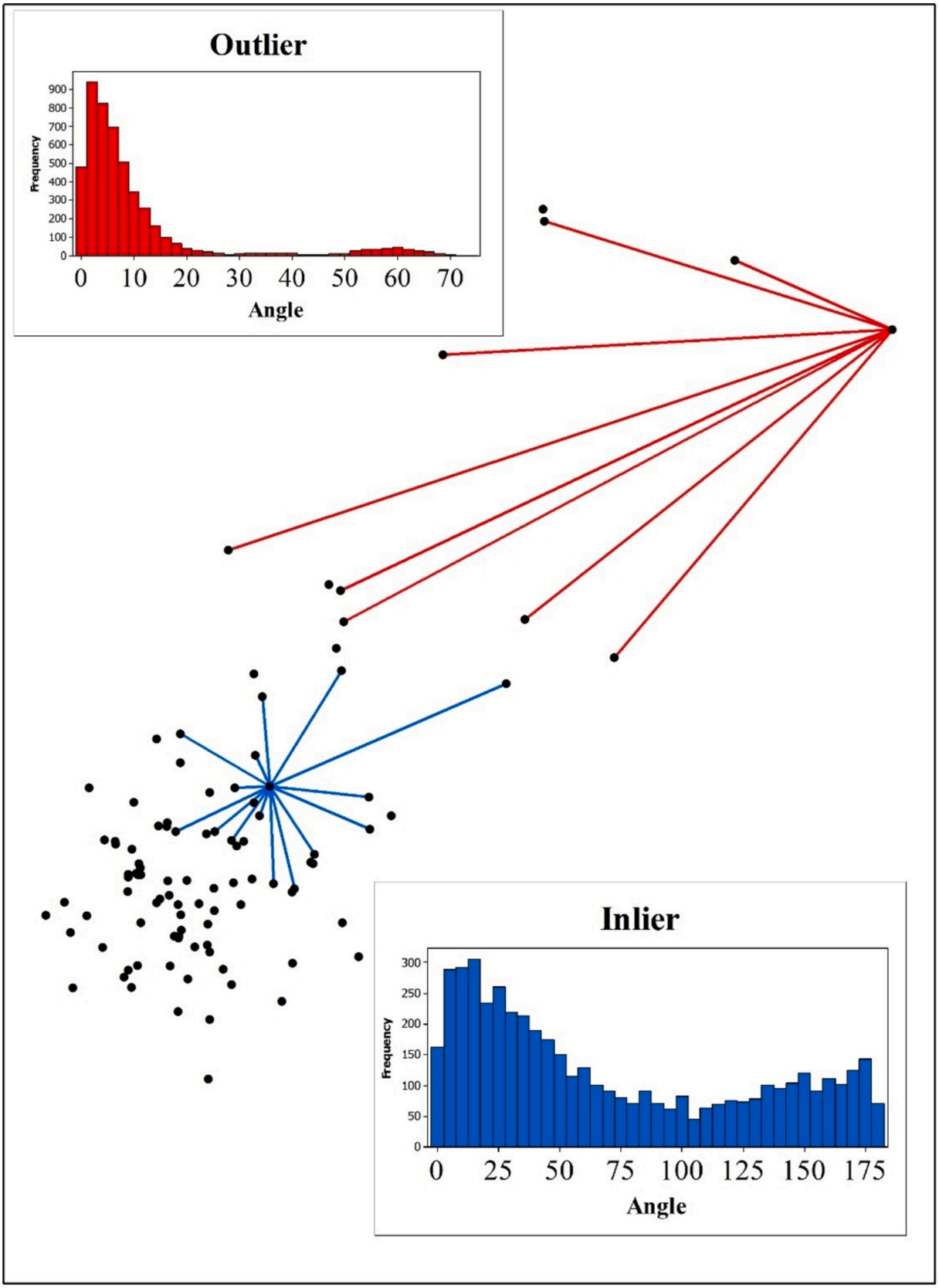

Fig. 3. Conceptual model for angle-based outlier detection (ABOD), featuring a two-dimensional example with Cu and Mo values. The inlier sample is shown in blue, while the outlier sample is in red. The histograms depict the range of calculated angles between inlier and outlier samples relative to other samples. (For interpretation of the references to colour in this figure legend, the reader is referred to the web version of this article.)

where ⟨AB, AC⟩ denotes the dot product of vectors AB and AC, and ||AB|| and ||AC|| represent the lengths of the respective vectors. In the ABOD method, the point with the highest rank stands out as the most extreme outlier. Following this, border points of the cluster are assigned ranks, with the lowest ranks reserved for the inner points of the cluster. ABOD achieves this by emphasizing the variance of angles as its primary criterion, with distance serving as a weighting factor. This methodology allows ABOD to efficiently detect outliers, even in datasets with high dimensions. Many outlier detection models require the user to specify parameters crucial to outcome of the approach. For unsupervised approaches, such requirements are always a drawback. Thus, a big advantage of ABOD is being completely free of parameters (Kriegel et al., 2008).

However, a drawback of the ABOD method is its time-consuming nature (order of $O(n^3)$), particularly due to the calculation of angles among all data points. Presented as an alternative to the original ABOD, the FastABOD approximation algorithm (Kriegel et al., 2008) utilizes k neighboring points with the highest weight in the variance calculation. This approach suggests that employing nearest neighbors could lead to a more accurate approximation, particularly in datasets with low dimensionality where distance carries more significance.

3. Results and discussion

3.1. Preprocessing

Geochemical dataset underwent a centered log-ratio transformation to address the constraints associated with compositional data (Aitchison, 1986). In the context of geochemical exploration of mineral deposits, two factors may influence the performance of outlier detection methods. The first factor is the selection of geochemical elements used in the outlier detection process, specifically those elements that provide information about the geochemical halo in the surficial dispersion from anomalous sources. The second factor is the size of the input feature space. For some outlier detection methods, such as distance-based or density-based methods, adding new dimensions can reduce efficiency due to the curse of dimensionality. Considering these factors, along with the time complexity of the ABOD method, two subsets of geochemical variables were chosen for this research. The first dataset comprised all analyzed trace and minor elements, including Ag, As, Au, B, Ba, Be, Bi, Cd, Ce, Co, Cr, Cu, Eu, Ga, Hf, Hg, Li, Mn, Mo, Nb, Ni, P, Pb, Sb, Sc, Sm, Sn, Th, Ti, V, Zn, and Zr. The second subset included only elemental commodities and key pathfinders, such as Ag, As, Au, Bi, Cu, Mo, Pb, Sb, and Zn. For instance, porphyry deposits have generated geochemical signatures of Cu, Au, Mo, and Bi, which are genetically, spatially, and temporally associated with intrusive rocks (Jamali et al., 2010; Maghsoudi et al., 2014). The decision to compare outlier detection performance using both the full set of elements and a selective subset of elemental commodities and key pathfinders was motivated by two key factors: evaluation of dimensionality sensitivity and model flexibility to adding new dimensions. By using the full set of elements, we aimed to assess how the methods respond to an expanded feature space, which includes additional trace elements that may sometimes explain the variability of dispersion halos around a mineral deposit. This allowed us to test the sensitivity of the methods to higher dimensionality and evaluate whether the inclusion of these elements influences the detection of geochemical anomalies. The second goal was to explore the flexibility of the methods in accommodating new dimensions, ensuring that they can adapt to variations in input variables without compromising their performance. This dual approach provides a more comprehensive understanding of the robustness of the methods across different geochemical scenarios, especially in cases where the full geochemical signature is not limited to traditionally recognized pathfinder elements.

3.2. ABOD and FastABOD

Both the original ABOD and FastABOD methods were employed on the two geochemical datasets. The outlier scores generated by ABOD and FastABOD were then interpolated using the inverse distance weighting (IDW) method, utilizing six neighboring samples. In regional-scale geochemical exploration, the sample catchment basin approach, which considers the upstream catchments as the zone of influence for stream sediment samples, has been shown to be superior to interpolation methods. However, research findings (e.g., Carranza, 2010; Shahrestani et al., 2019) comparing the continuous and discrete viewpoints of stream sediment samples suggest that IDW method can also identify geochemical anomalies that are often valid and spatially correlated with known mineral deposits.

Fig. 4 displays the anomaly maps generated by applying the ABOD method using all elements and primary commodity elements, comparing the original ABOD algorithm with its approximation, FastABOD. To classify the anomaly maps, thresholds were selected based on the 1st, 2nd, 3rd, and 4th quantiles. When examining the patterns of geochemical anomalies from the four ABOD implementations, the scatter plots of anomaly scores for ABOD_All, ABOD_Selective, FastABOD_All, and FastABOD_Selective (Fig. 5) indicate that both ABOD and FastABOD produce similar scores when only a subset of elements is used. However, significant discrepancies arise when ABOD and FastABOD are applied to all 32 elements, highlighting the influence of considering only the k nearest neighbors. As the number of input variables decreases, the difference between ABOD and FastABOD scores diminishes. In other words, with fewer geochemical variables, ABOD and FastABOD produce more similar anomaly scores compared to when they are applied to a high-dimensional feature space with many geochemical variables.

To evaluate the effectiveness of four different implementations of the ABOD method for comparing four geochemical anomalies (ABOD_All, ABOD_selective, FastABOD_All, and FastABOD_Selective), a different procedure was utilized (Table 1). The procedure involved determining the number of mineral occurrences within each class. The process began with calculating the number of pixels in each quantile (Qi, where i = [1, 4]) using ArcGIS. Subsequently, known deposits within each Qi were identified. The quartile threshold values were chosen to ensure that all four classes had approximately similar areas, enhancing the contribution of detected known occurrences in each Qi. Using quantiles to map geochemical anomalies offers advantage especially when dealing with outlier scores from different methods with varying distributions. Quantiles divide the data into equal parts based on ranking rather than absolute values, making them independent of the underlying distribution. This ensures that each quartile contains a consistent proportion of the data, regardless of whether the scores follow a normal, skewed, or multimodal distribution (e.g., Liu et al., 2024; Wang and Zuo, 2022). The score assigned to each class was based on the proportion of detected known deposits relative to the area of that class. Two benchmark values were considered for comparison: the ratio of the number of delineated mineral occurrences to the area of class Q4 and the merged values of Q3 and Q4 classes. In terms of effectiveness in delineating known mineral occurrences, ABOD_Selective ranked highest when considering only Q4, capturing around 61 % of all known occurrences in the highest score class. On the other hand, FastABOD_Selective showed superior anomaly delineation performance when considering integrated Q3 and Q4 classes. Moreover, it was observed that when focusing on limited main element commodities, ABOD anomaly classes more effectively delineated known mineral occurrences compared to considering all elements. This difference may be due to the influence of additional elements affected by factors unrelated to mineralization. For example, lithological variations play a significant role in elemental distribution, potentially reducing the efficacy of anomaly detection methods in highlighting mineralization-related geochemical signals. In multivariate anomaly delineation using angle-based outlier detection with a limited number of variables, despite the time-consuming nature of the original ABOD

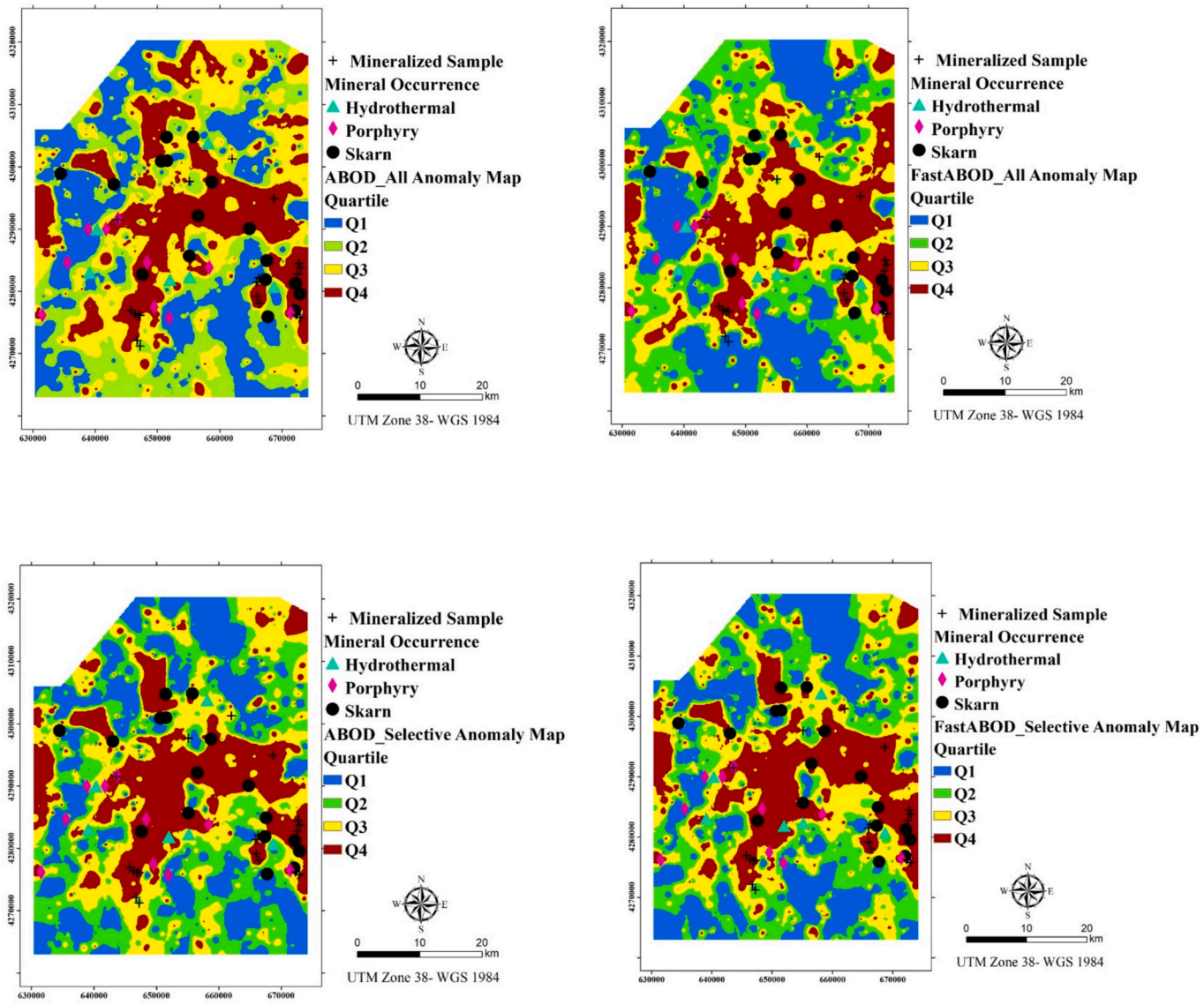

Fig. 4. Anomaly maps of ABOD_All, ABOD_Selective, FastABOD_All, and FastABOD_Selective classified based on quartile.

method, it is recommended to use ABOD over the FastABOD approach (Kriegel et al., 2008).

Comparing the four anomaly maps can also be done using receiver operating characteristic (ROC) curves (Fawcett, 2006). ROC curves illustrate the balance between the true positive rate (TPR) and the false positive rate (FPR) at different decision thresholds. The top left corner of the ROC space corresponds to an ideal classifier with coordinates (0,1). The area under the ROC curve provides a comprehensive evaluation of performance across all threshold settings, making it a crucial metric for assessing the effectiveness of geochemical anomaly detection models. Constructing ROC curves necessitates labeled data. In the context of unsupervised anomaly detection in geochemical exploration, the positions of known mineral deposits can serve as labeled data. In the current geochemical survey, stream sediment analysis was followed by an anomaly verification stage involving the examination of rock samples from the study area. The identified mineralized samples, along with the locations of known mineral occurrences, can be used to create ROC curves - one for known mineral deposits and another for mineralized samples. Positive samples in each dataset correspond to pixels where known deposits and mineralized samples were identified, while negative samples were randomly selected from the study area. These negative samples serve as a baseline for evaluating the performance of an anomaly detection method. The comparison between true positives and randomly selected false positives helps in assessing how effectively the method distinguishes mineral deposits from random noise. These positive and negative scores were then leveraged to generate ROC curves for each detection method. Fig. 6 displays the ROC curves for each anomaly detection method based on the datasets of known deposits and mineralized samples. When using known mineral occurrences as labeled data, similar performance is observed across the four approaches, with slightly better performance noted in FastABOD_All and ABOD_Selective. On the other hand, when using mineralized samples as the labeled data, a notable distinction is evident, highlighting the superiority of the selective approach over considering all trace and minor elements. This reaffirms the effectiveness of the selective approach in prediction-area analysis (Table 1).

3.3. Feature importance

To delve deeper into the anomaly scores produced by the four variations of ABOD, an evaluation of the impact of each clr-transformed elemental value on the anomaly scores was conducted using random forest regression. The analysis employed a forest consisting of 100 trees, each with 2 splits, and a fixed random state of 42 to ensure

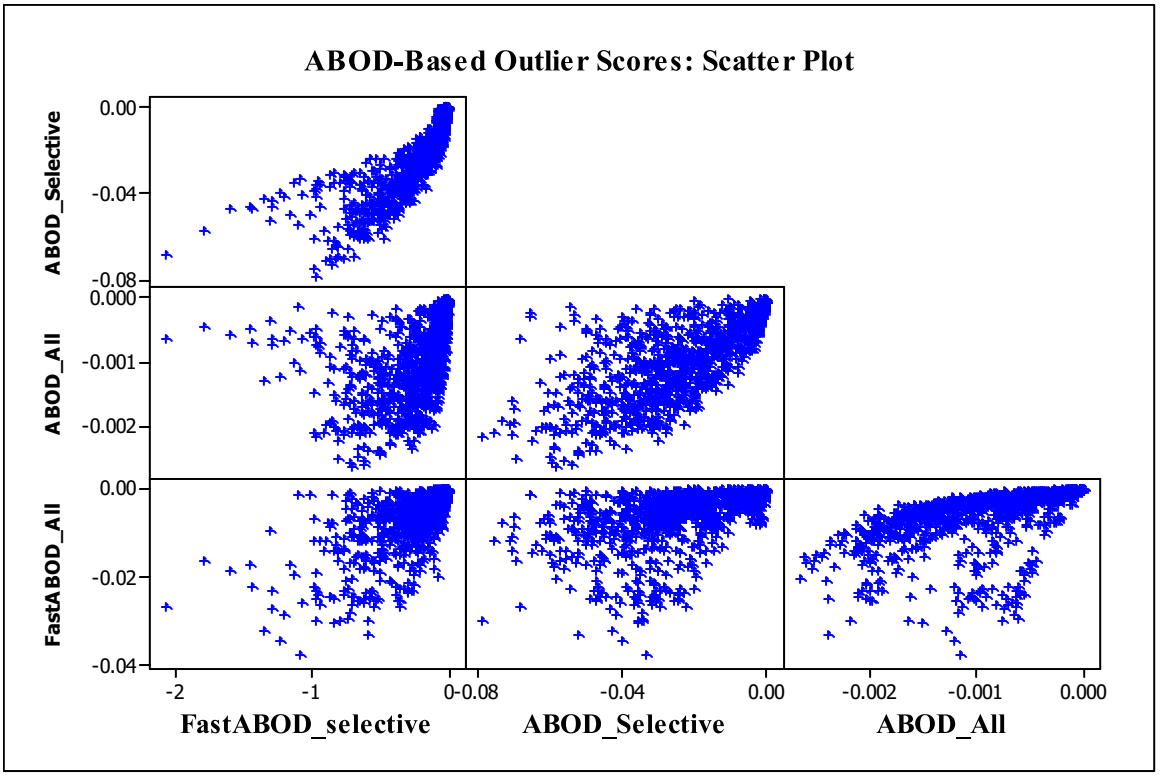

Fig. 5. Scatter plots of anomaly scores resulting from ABOD_All, ABOD_Selective, FastABOD_All, and FastABOD_Selective variations.

Table 1
Comparing the effectiveness of ABOD_All, ABOD_Selective, FastABOD_All, and FastABOD_Selective in identifying known mineral occurrences in the study area.

Method	A	B	C	D	E	F	G
ABOD_All	Q1	19,394	4	12.12	25.11	0.48	
	Q2	19,556	6	18.18	25.32	0.72	
	Q3	19,262	8	24.24	24.94	0.97	
	Q4	19,032	15	45.45	24.64	**1.84***	**2.81****
ABOD_Selective	Q1	19,584	3	9.09	25.35	0.36	
	Q2	19,826	5	15.15	25.67	0.59	
	Q3	19,170	5	15.15	24.82	0.61	
	Q4	18,664	20	60.61	24.16	**2.51***	**3.12****
FastABOD_All	Q1	19,405	3	9.09	25.12	0.36	
	Q2	19,283	5	15.15	24.96	0.61	
	Q3	20,351	9	27.27	26.35	1.04	
	Q4	18,205	16	48.48	23.57	**2.06***	**3.10****
FastABOD_Selective	Q1	19,714	5	15.15	25.52	0.59	
	Q2	20,092	2	6.06	26.01	0.23	
	Q3	18,934	10	30.30	24.51	1.24	
	Q4	18,504	16	48.48	23.96	**2.02***	**3.26****

A: Threshold, B: Number of pixels in each class, C: Number of deposits in each class, D: Relative number of occurrences (%) in each class, E: Relative area (%) of each class, F: D/E, G: Sum of D/E values in Q3 and Q4 classes.* and ** denote area-prediction efficiency indices in Q4 and (Q3+Q4) classes, respectively.

reproducibility. In the case of ABOD_All (Fig. 7), the contributions of Sb, Th, Be, Nb, Li, As, and Au were notably highlighted. These associations can be partially attributed to hydrothermal mineralization processes in the study area. For FastABOD_All (Fig. 7), the analysis emphasized the contributions of Ni, Th, Hf, Cr, Eu, Li, Sm, and Be. These elements (e.g., Ni and Cr) suggest that the FastABOD_All scores may be influenced by lithology. The random forest analysis revealed similar element contributions in the anomaly scores of ABOD_Selective and FastABOD_Selective. In both cases, the contributions of Sb, Au, and As were prominently highlighted. However, in addition to Sb, Cu played a dominant role in the FastABOD_Selective scores. This could be one of the reasons why the FastABOD_Selective approach is preferred for delineating geochemical signals from both copper-rich mineralization types like porphyry and skarn copper deposits, as well as hydrothermal mineralization in the study area.

3.4. ABOD, PCA, and ICA

Another approach for examining the effectiveness of the ABOD method in delineating geochemical anomalies is to compare the ABOD anomaly maps with dimension reduction methods that highlight the main geochemical patterns. In this paper, independent component analysis (ICA) is applied, building on the complementary work conducted by Iwamori and Albarède (2008), Iwamori et al. (2010), Yu et al. (2007, 2012), Zhang et al. (2007), Liu et al. (2014), Yang and Cheng (2015 a, b) and Shahrestani et al. (2024) where ICA was used for geochemical interpretations. ICA was selected as a benchmark in this study due to its ability to extract statistically independent sources from

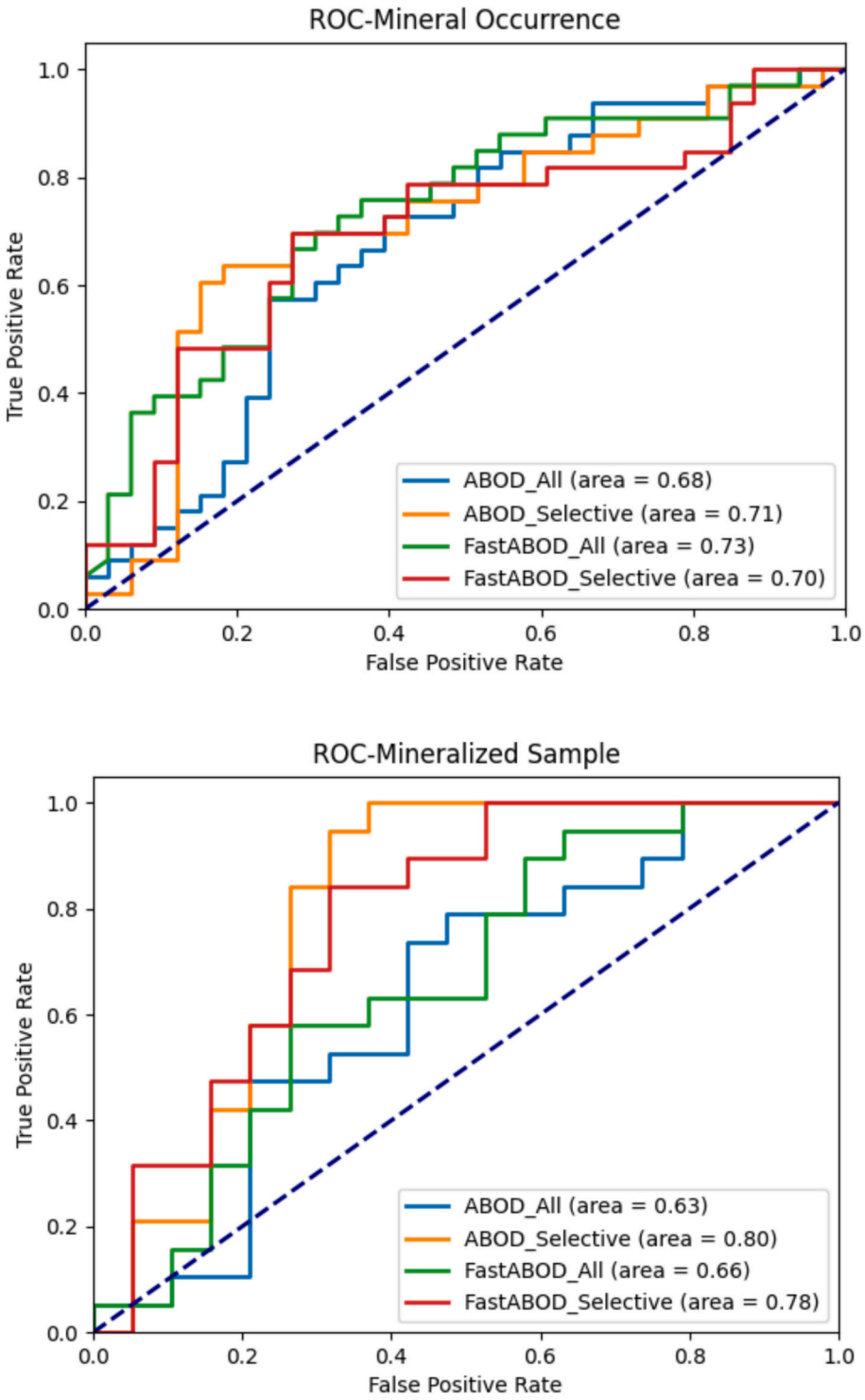

Fig. 6. Receiver operating characteristic (ROC) curves of ABOD_All, ABOD_Selective, FastABOD_All, and FastABOD_Selective methods based on the known mineral occurrences (up) and mineralized samples (down).

multivariate geochemical data, which is crucial for exploring geochemical anomalies (Shahrestani et al., 2024). ICA uses higher-order statistics, such as kurtosis, to identify non-Gaussian independent components, making it particularly suitable for geochemical datasets where different processes—like mineralization, weathering, and hydrothermal alteration—contribute overlapping signatures. In geochemical exploration, the assumption of statistical independence allows ICA to better distinguish between multiple geochemical sources, revealing hidden structures that represent distinct geochemical processes. In this study, ICA identified components highlighting elements such as As, Sb, Au, Cu, and Mo, which are key indicators of mineralization in the study area. This ability to isolate independent geochemical signals offers a more detailed interpretation of the variability in geochemical halos, as ICA captures the contributions of specific processes to the observed anomalies. When compared to ABOD, which identifies outliers based on variations in local density within high-dimensional space, ICA offers a complementary approach. While ABOD detects anomalous points by analyzing geometric deviations, ICA isolates the underlying

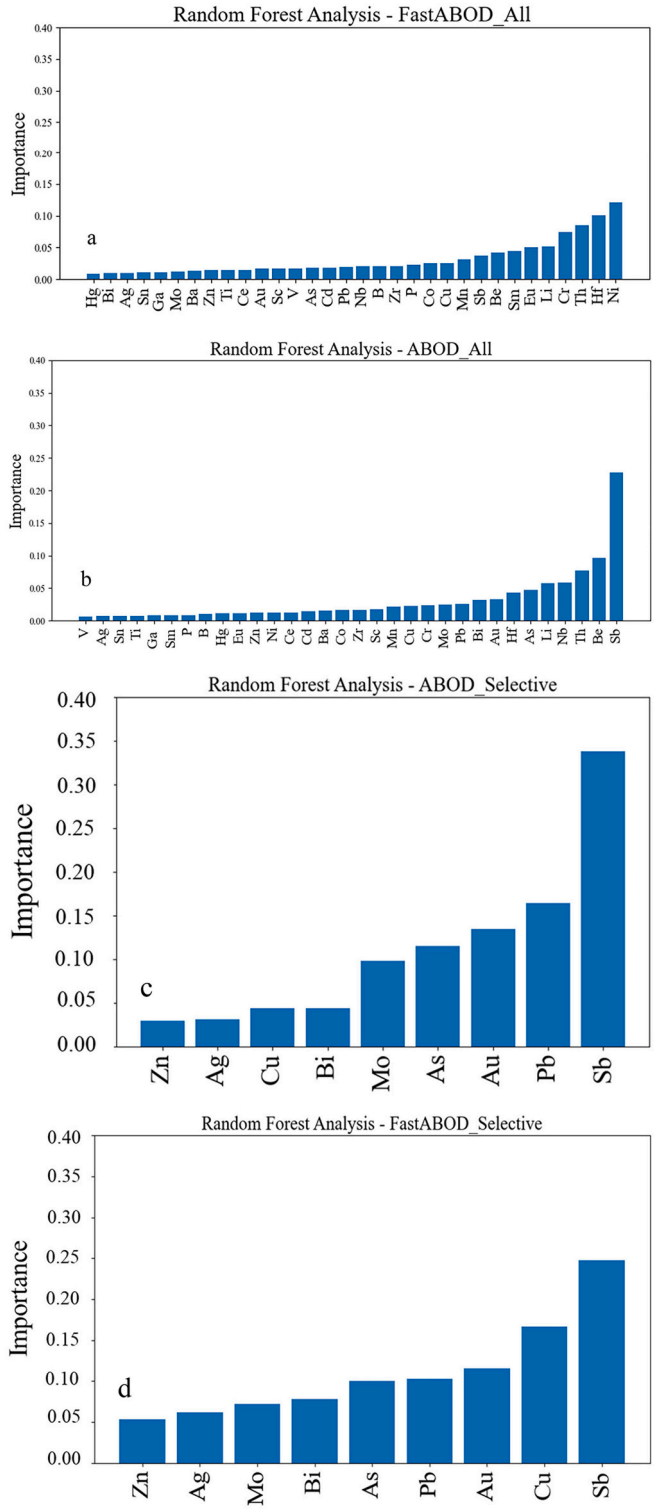

Fig. 7. The relative importance of clr-transformed elemental values in the resulting anomaly scores generated by the ABOD_All (a), ABOD_Selective (b), FastABOD_All (c), and FastABOD_Selective (d) variations.

independent sources of geochemical variability. The comparison between ICA and ABOD is technically justified because both methods provide distinct yet complementary perspectives on anomaly detection: ABOD focuses on identifying outliers based on the spatial distribution of points, whereas ICA uncovers independent geochemical patterns that may reflect key geological processes. In the context of geochemical exploration, where multiple independent sources contribute to observed variability, ICA serves as an effective benchmark, helping to assess how well ABOD captures anomalies related to these independent processes. The mathematical presentation of ICA can be found in the aforementioned references. ICA also surpasses PCA by focusing on statistically independent and non-Gaussian components rather than just maximizing variance. ICA uses higher-order statistics like kurtosis to measure non-Gaussianity and independence, capturing complex dependencies that PCA overlooks. This allows ICA to reveal underlying structures and sources in the data more effectively. Unlike PCA, which assumes linearity and decorrelation, ICA identifies components that are truly independent, providing more accurate and interpretable results for complex datasets with non-linear relationships (e.g., Shahrestani et al., 2024; Yang and Cheng, 2015). In this study, the FastICA algorithm was performed using parameters recommended by Hyvärinen (1999), including the application of the tanh function and symmetric decorrelation. To maximize the contrast between the information provided by each independent component, five ICs were selected, although there is no limitation on selecting up to nine ICs. Table 2 presents the loadings of elements in each of the five ICs. IC1 highlights the contribution of As and Sb. In IC2, Au, Cu, and Mo are indicated, which can be considered influential factors in delineating mineralization in the study area. No element shows high loadings in IC3, and this is also the case for IC4, except for Pb, which shows a high loading. As, Au, and Sb show high loadings in IC5, making it a good component for delineating Au-bearing mineralization in the study area.

Fig. 8 displays the interpolated maps for the scores of five ICs. As indicated by the loadings, a clear alignment is observed between known mineral occurrences and the anomaly maps for IC2 and IC5. To assess the effectiveness of ICA in detecting mineralization-related anomalies, an ROC curve analysis was conducted using the five ICs and two higher-performing ABOD methods: ABOD_Selective and FastABOD_Selective. Among all ICs, IC2 shows a performance comparable to these ABOD variants, as evidenced by the area under curve values: IC2 (0.72), ABOD_Selective (0.71), and FastABOD_Selective (0.70). Further comparison between IC2, IC5, ABOD_Selective, and FastABOD_Selective can be made using mineralized samples as label data (Fig. 9). Similar to the case with mineral occurrence, the IC2 score map provides superior performance in highlighting known mineralized zones (Fig. 10). IC5 also effectively delineates mineralized areas.

In Table 3, the overall effectiveness of the ABOD method in delineating geochemical anomalies across all three mineralization types is compared and contrasted. However, based on the classified geochemical anomaly maps (Fig. 4), the efficiency of ABOD varies among the porphyry, hydrothermal, and skarn mineral occurrences. ABOD_Selective, identified as the best outlier detection variant, successfully places 76 % and 70 % of skarn, porphyry mineral occurrences in the Q4 anomaly class, respectively. Notably, ABOD struggled to delineate geochemical anomalies associated with hydrothermal deposits (16 %). This may be due to the smaller geochemical halos around these deposits relative to porphyry or skarn deposits, given the sampling density of the geochemical survey, or the complexity of the geochemical associations between elemental variables that the ABOD approach could not effectively capture. To improve the efficiency of ABOD in identifying

Table 2
ICA loadings of geochemical variables on five ICs emerging from ICA.

	IC1	IC2	IC3	IC4	IC5
As	**0.463**	0.166	−0.568	−0.075	**0.207**
Au	−0.034	**0.430**	−0.011	−0.051	**0.756**
Bi	0.033	0.285	0.032	−0.088	0.011
Cu	−0.056	**0.423**	0.012	−0.075	0.021
Mo	−0.074	**0.603**	−0.081	−0.115	−0.062
Pb	0.018	0.277	−0.056	**0.848**	0.047
Sb	**0.594**	0.234	−0.015	−0.073	**0.176**
Zn	0.010	−0.037	0.045	−0.066	−0.049

Bold values indicate elements with high loading values in each IC.

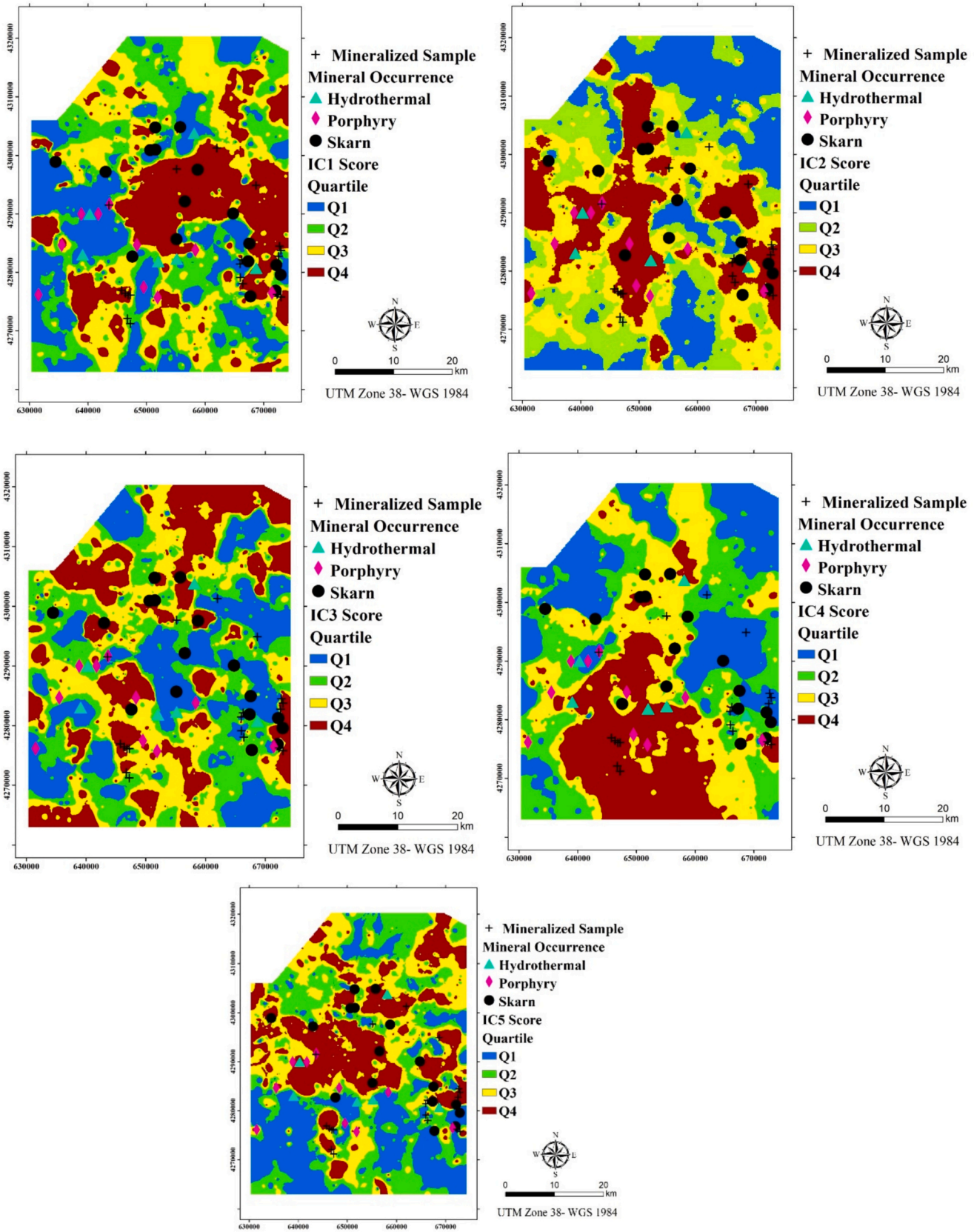

Fig. 8. Spatial distribution of five ICA scores on clr-transformed multivariate geochemical data.

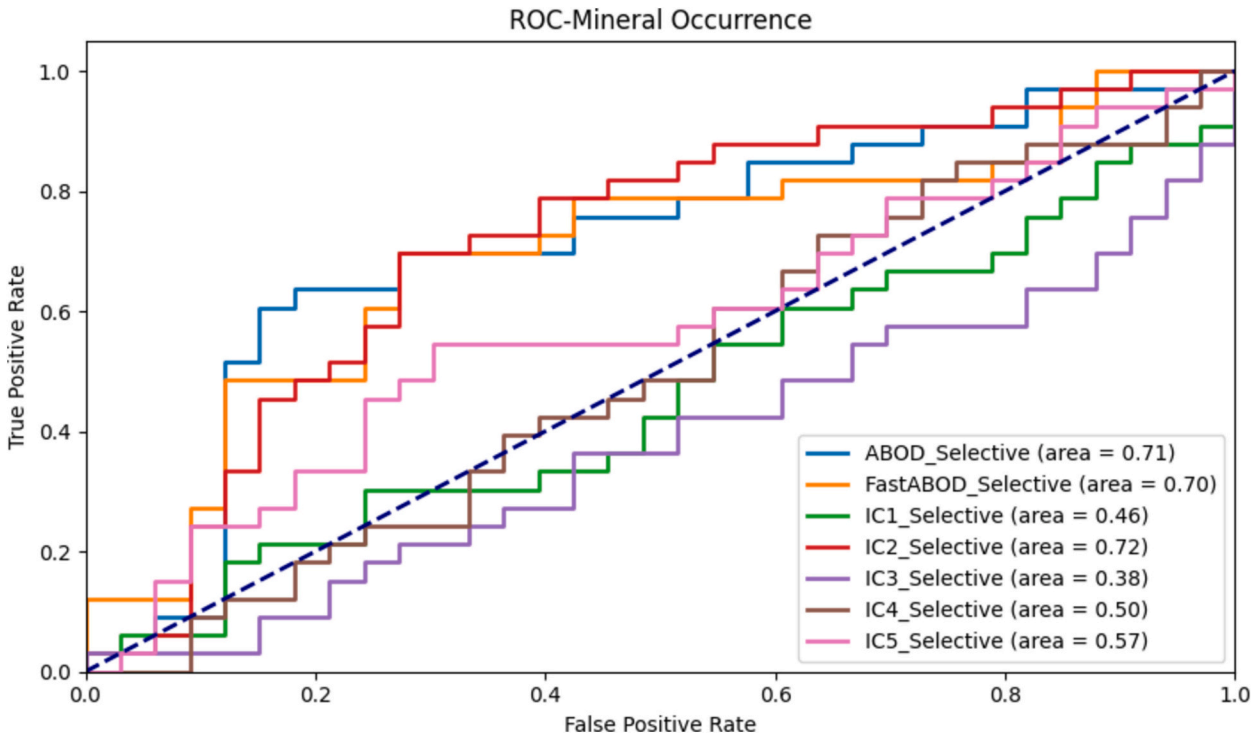

Fig. 9. Receiver operating characteristic (ROC) curves of ABOD_Selective, FastABOD_Selective variations and five ICs methods based on the known mineral occurrences.

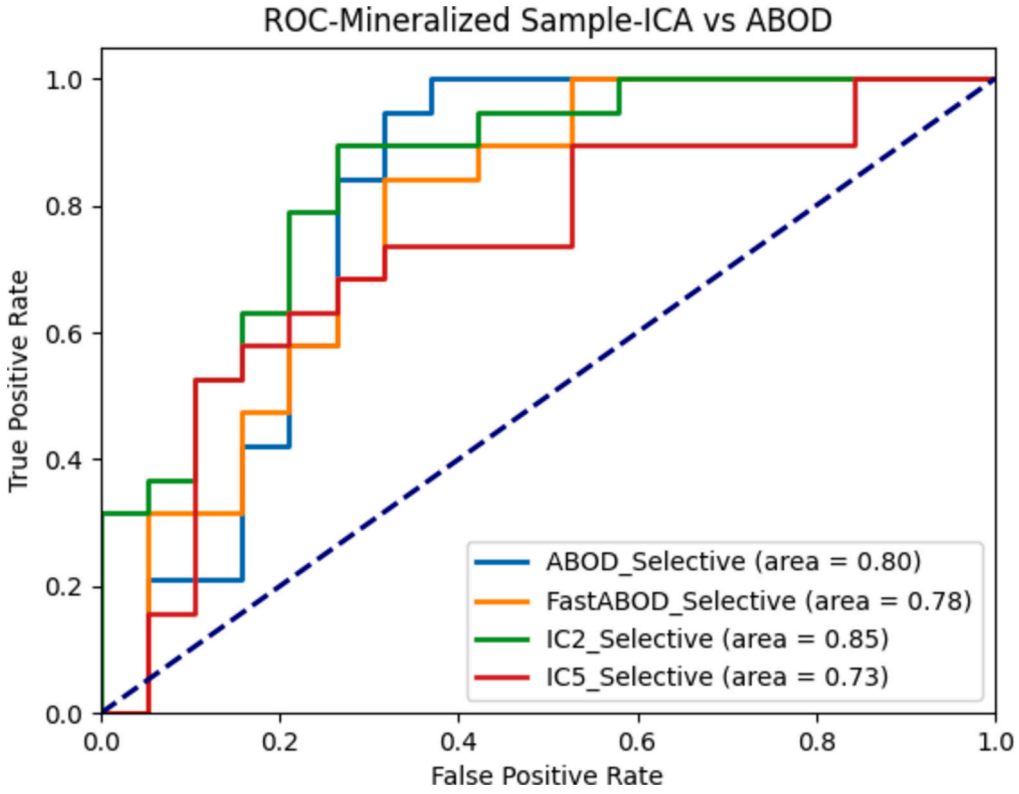

Fig. 10. Receiver operating characteristic (ROC) curves of ABOD_Selective, FastABOD_Selective methods and IC2 and IC5 anomaly maps based on the mineralized samples.

geochemical anomalies, PCA was performed on the entire dataset, leading to the selection of eight principal components based on the scree plot (not displayed here). FastABOD was then applied to this new feature space, with the resulting outlier scores from FastABOD_PCA illustrated in Fig. 11 The effectiveness of the FastABOD_PCA method in detecting geochemical anomalies is compared to other methods in Table 3. This

Table 3
Efficiency of IC2, IC5, ABOD_Selective, and FastABOD_Selective methods within the Q4 class of score maps in delineating skarn, porphyry, and hydrothermal mineral occurrences.

	IC2		IC5	
Deposit type	Number of deposits in Q4	% (out of 19)	Number of deposits in Q4	% (out of 10)
Skarn	**7** (17)	37	**7** (17)	70
Porphyry	9 (10)	47	**2** (10)	20
Hydrothermal	3 (6)	16	1 (6)	10
Total (out of 33)	19	58	10	31

	ABOD_Selective		FastABOD_Selective	
Deposit type	Number of deposits in Q4	% (out of 20)	Number of deposits in Q4	% (out of 16)
Skarn	11 (17)	55	8 (17)	50
Porphyry	**7** (10)	35	6 (10)	38
Hydrothermal	2 (6)	10	2 (6)	13
Total (out of 33)	20	61	16	49

	FastABOD_PCA	
Deposit type	Number of deposits in Q4	% (out of 25)
Skarn	13 (17)	52
Porphyry	7 (10)	40
Hydrothermal	5 (6)	20
Total (out of 33)	25	76

approach successfully delineated the majority of mineral deposits, achieving a significant improvement in detecting hydrothermal occurrences when both unsupervised feature selection techniques were applied concurrently. The FastABOD_PCA anomaly map indicated that 76 % of the mineral deposits were identified in Q4, representing the highest efficiency among the various methods employed.

Based on the loadings from ICA, Mo is the most influential element for the anomaly score in IC2, followed by Cu and Au. In IC5, Au has a substantial impact on the component score, whereas As and Sb contribute relatively less. This sparked interest in determining whether the IC2 and IC5 score maps could differentiate between various types of mineral occurrences in the research area. Subsequently, the number of skarn, porphyry, and hydrothermal mineral occurrences within the Q4 class of the IC2, IC5, ABOD_Selective, and FastABOD_Selective score maps were tabulated (Table 3). Among these maps, 19, 10, 20, and 16 known mineral occurrences fell into the Q4 classes of the IC2, IC5, ABOD_Selective, and FastABOD_Selective maps, respectively. The percentage of each mineralization type among all known occurrences in the Q4 class was also calculated. A similar pattern was observed in the relative percentages of delineated skarn, porphyry, and hydrothermal deposits in the ABOD_Selective and FastABOD_Selective maps. However, distinctive characteristics were noted in the IC2 and IC5 maps. IC2 effectively outlined porphyry Cu-Mo deposits, whereas IC5 highlighted skarn mineralization efficiently. This illustrates the strength of ICA, where each IC can spotlight unique geochemical patterns compared to other ICs. A combined consideration of effective ICs, such as IC2 and IC5 in this case, can improve the chances of identifying more mineralized zones within a study area.

To achieve a better understanding of the efficiency of IC2 and IC5 and ABOD methods in outlining the sources of mineralization, mineralized samples significantly enriched in Cu and Au are selected. Separate ROC analyses are conducted to confirm the role of the relative loading of

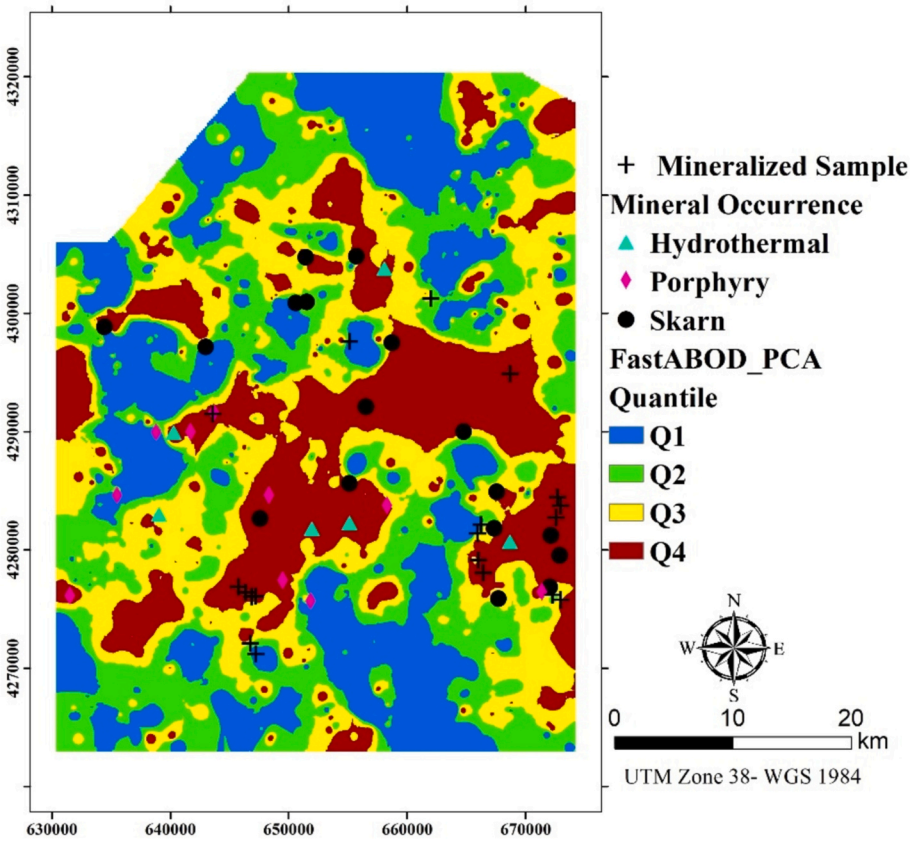

Fig. 11. Anomaly map of FastABOD_PCA scores classified based on quartile.

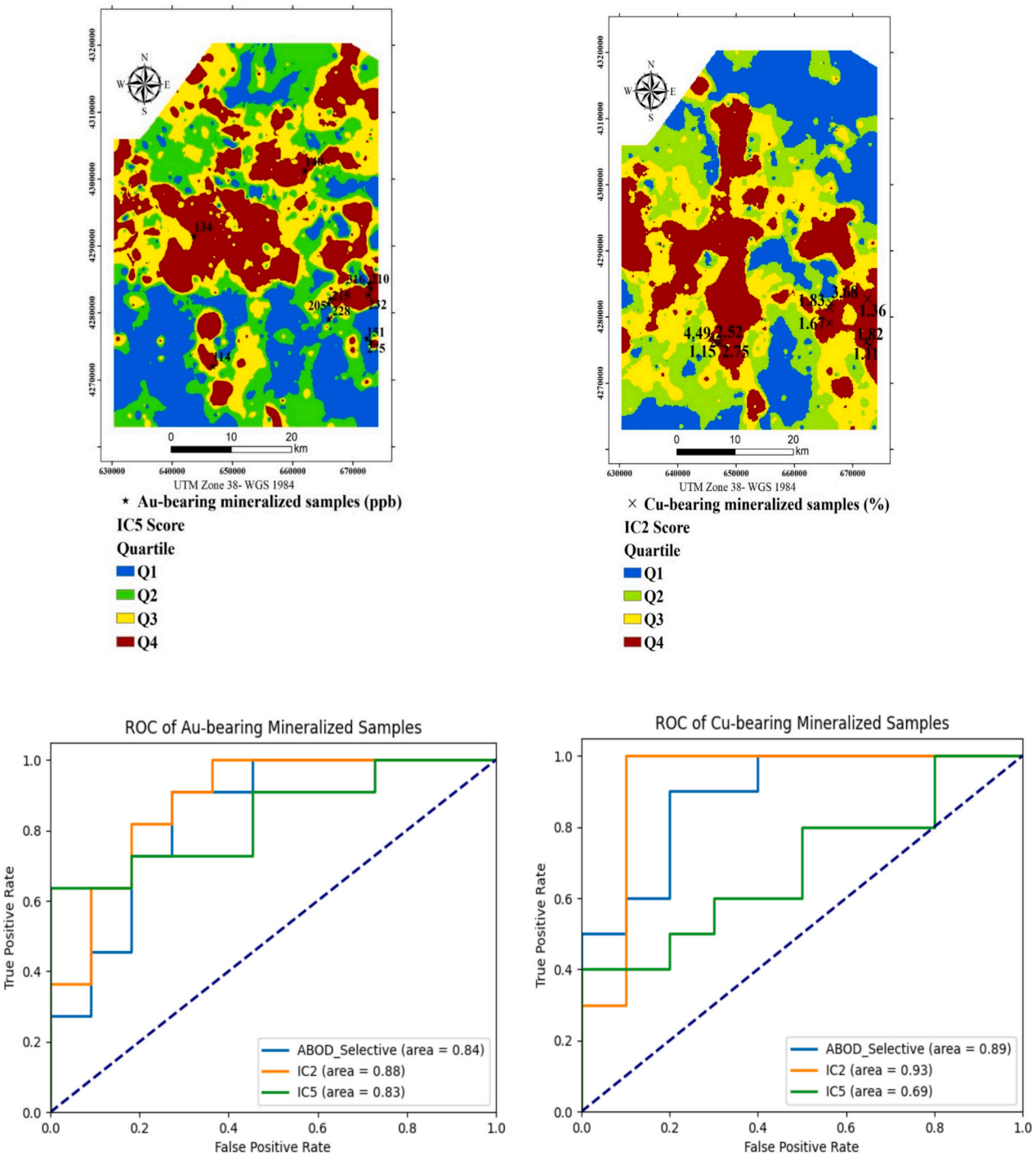

Fig. 12. Receiver operating characteristic (ROC) curves of ABOD_Selective approach and IC2 and IC5 anomaly maps based on the mineralized samples significantly enriched in Au (left) and Cu (right).

Cu and Au in the anomaly scores (Fig. 12). Despite fewer known mineral occurrences being delineated in the Q4 anomaly class by the IC5 score map, it is very effective in outlining Au-bearing mineralized zones, as evidenced by delivering comparable area under curve values to ABOD and IC2 maps. The sensitivity of IC2 scores to Cu values can be observed in Fig. 12. The superiority of the IC2 score map in highlighting mineralized zones enriched in Cu is approved by ROC. However, a relatively balanced successfulness in delineating Au and Cu-bearing zones is displayed by the ABOD method, signifying that if there are diverse sources of mineralization enriched by different element commodities, the ABOD method can identify them.

3.5. ABOD and other outlier detection methods

To assess the effectiveness of ABOD in geochemical anomaly detection, a comparative study is conducted between ABOD and other outlier detection methods, including LOF, kNN, and the isolation-based nearest neighbor ensemble (iNNE), all of which focus on identifying local outliers. Fig. 13 presents the geochemical anomaly maps produced by the four outlier detection methods. As expected, LOF demonstrates a different spatial distribution of geochemical anomalies due to its basis on contrasting the local density of the target sample with the local densities of its neighbors. The other three methods, including kNN,

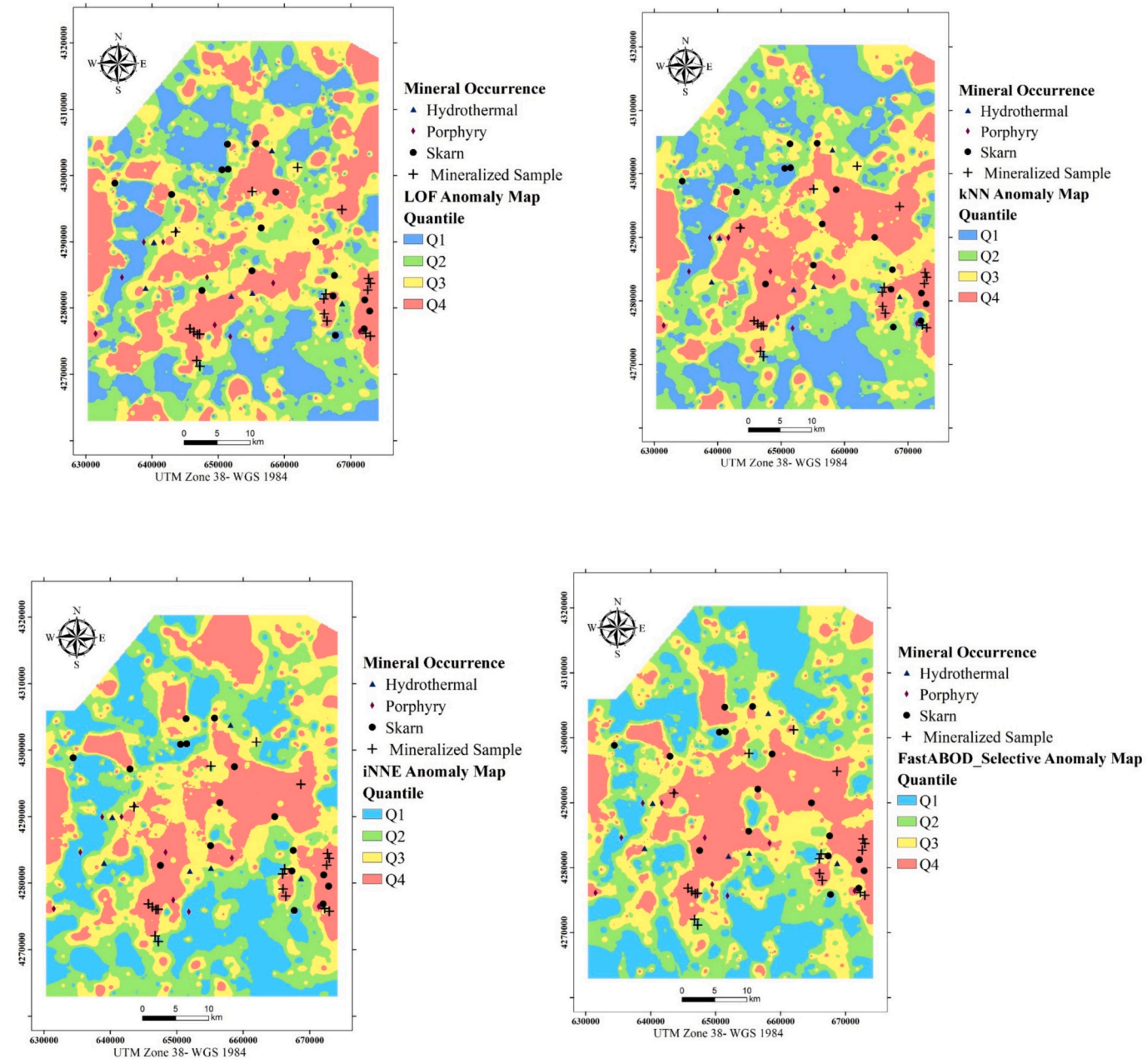

Fig. 13. Anomaly maps displaying interpolated outlier scores from LOF, kNN, iNNE, and FastABOD_Selective, classified according to quartiles.

iNNE, and FastABOD, which apply discrimination criteria based on a specific number of neighboring samples (distance, isolation, and angle-distance), show relatively similar spatial distributions of geochemical anomalies. ROC curves using mineral occurrences and mineralized samples as validation points are constructed to compare the efficiency of the four anomaly maps. In both cases, there is no considerable difference in the area under the curve values among the four methods, although the FastABOD algorithm demonstrates a slight superiority, particularly when mineralized samples are considered as validation points (Fig. 14). This result indicates that, despite ABOD utilizing a straightforward criterion—namely, the variance of angles between samples as vectors in feature space—it remains effective for geochemical anomaly detection.

Considering the two different geochemical data subsets with 9 and 32 dimensions, ABOD proves effective in detecting anomalies by leveraging the angles between data points, which provides a more robust attribute than distance and density alone. This makes ABOD suitable for complex geochemical datasets with multiple variables. Its ability to work without the need for specific parameter tuning or a training phase simplifies its application and reduces the risk of user-induced bias. The FastABOD variant further enhances outlier detection by limiting the local region of the target point, offering a balanced approach. While ABOD excels in identifying mineralization-related anomalies and is less susceptible to dimensionality issues compared to methods like LOF, it is computationally expensive for large datasets due to the need to calculate angles between all pairs of points. Thus, FastABOD stands out as a strong candidate for analyzing high-dimensional multivariate geochemical datasets. In scenarios with high-dimensional data, angle-based approach of ABOD can outperform density-based methods like LOF, which may struggle with the curse of dimensionality. The advantage of ABOD lies in its parameter-free approach, making it preferable over methods such as LOF and iForest, which require meticulous parameter tuning. However, for very large datasets, the computational complexity of ABOD might be a drawback, making computationally efficient methods like iForest more suitable.

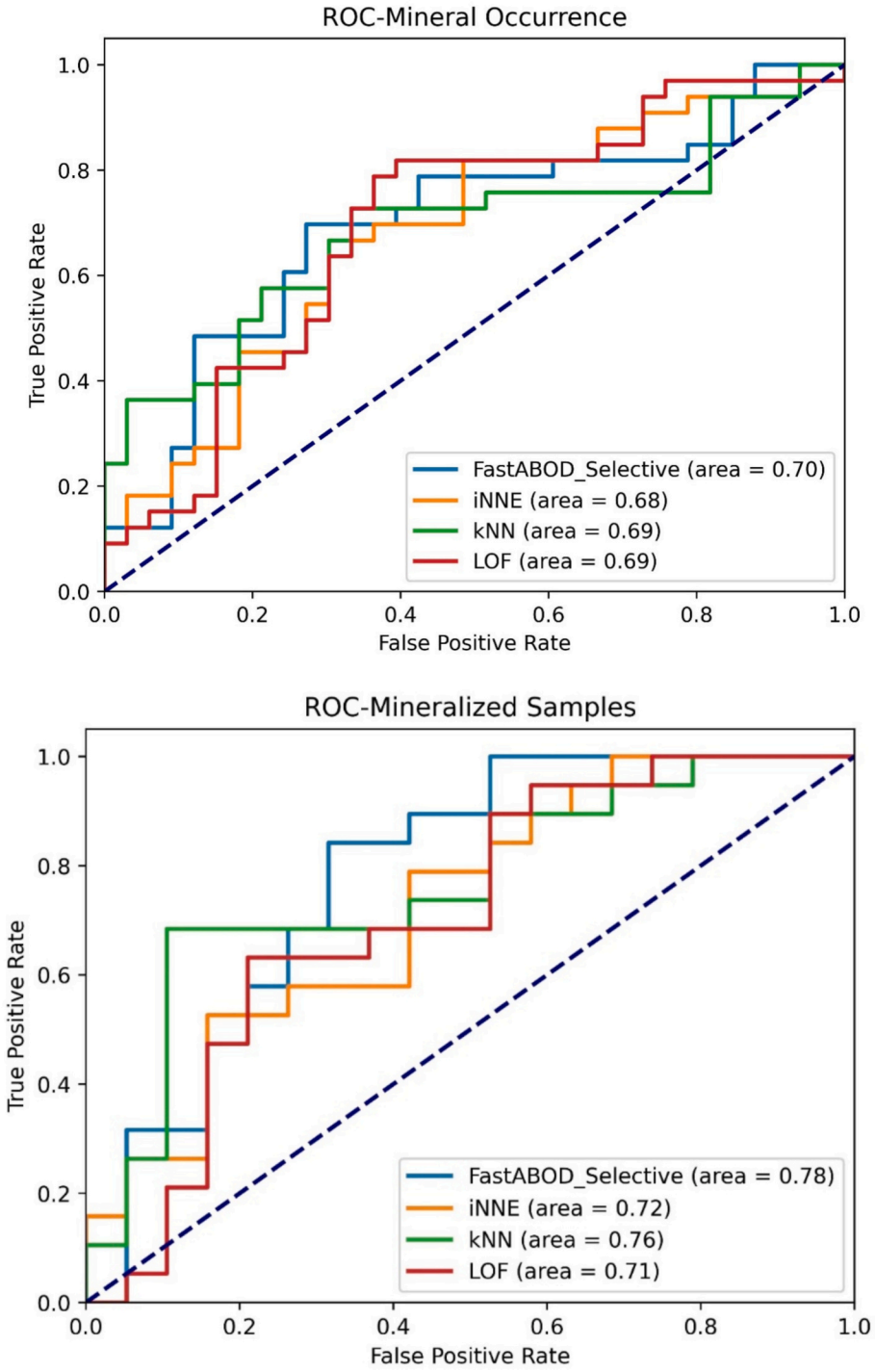

Fig. 14. Receiver operating characteristic (ROC) curves evaluating the efficiency of LOF, kNN, iNNE, and FastABOD_Selective in identifying geochemical anomalies related to mineralization in the study area (up: Mineral occurrences and down: Mineralized samples).

Considering the two different geochemical data subsets with 9 and 32 dimensions, ABOD effectively detects geochemical anomalies in high-dimensional data by considering a more robust attribute (i.e., the angles between data points) than distance and density, which makes it suitable for complex geochemical datasets with multiple variables. Accordingly, considering only the angle and distance, ABOD does not require the tuning of specific parameters or a training phase, simplifying its application and reducing the risk of user-induced bias in geochemical data analysis. Additionally, a potential characteristic of ABOD in limiting the local region of the target point (FastABOD) offering a balanced approach to outlier detection. In this research, although nine variables including main elemental commodities and their pathfinder are incorporated in both ABOD and its fast version, the approach effectively delineates mineralization-related geochemical anomalies. However, the original version of ABOD is computationally expensive, especially for large datasets, as it requires calculating the angles between all pairs of points, which can limit its scalability and speed.

4. Conclusions

1. The research demonstrates that the angle-based outlier detection (ABOD) method, particularly when focusing on key elemental

commodities and pathfinders, proves to be effective in detecting anomalies in high-dimensional geochemical datasets. Selective subsets of variables lead to more accurate anomaly detection compared to using all trace and minor elements, emphasizing the importance of dimensionality reduction for successful anomaly identification. Consequently, ABOD_Selective demonstrated a high success rate in detecting known mineral deposits, with 76 % of skarn and 70 % of porphyry occurrences classified in the highest anomaly category.
2. The research demonstrates the effectiveness of independent component analysis (ICA), particularly IC2 and IC5, in delineating porphyry Cu-Mo deposits and skarn mineralization, respectively. This comparative analysis offers valuable insights into the complementary nature of ICA and ABOD in identifying mineralization sources enriched in elements such as Cu and Au.
3. The comparison of LOF, kNN, iNNE, and ABOD indicates that LOF presents distinct anomaly distributions due to its local density approach, while kNN, iNNE, and FastABOD produce similar maps based on distance and angle-based methods. ROC analysis reveals that FastABOD has a slight advantage in performance, particularly in detecting mineralized samples.
4. The study underscores the advantages of ABOD in detecting outliers in high-dimensional data, emphasizing its insensitivity to data scale and ability to capture local outliers. However, limitations such as computational complexity, sensitivity to noise, and potential false positives must be considered when utilizing the method in mineral exploration studies.

CRediT authorship contribution statement

Shahed Shahrestani: Writing – review & editing, Writing – original draft, Visualization, Validation, Software, Methodology, Investigation, Formal analysis, Conceptualization. **Ioan Sanislav:** Writing – review & editing, Writing – original draft, Visualization, Validation, Supervision, Methodology, Investigation, Formal analysis, Conceptualization.

Declaration of competing interest

The authors declare that they have no known competing financial interests or personal relationships that could have appeared to influence the work reported in this paper.

Acknowledgments

The authors extend their gratitude to the Geological Survey of Iran for generously providing the regional stream sediment geochemical data from the Varzaghan area, which made a significant contribution to this study.

Data availability

The data that has been used is confidential.

References

Aggarwal, C.C., Hinneburg, A., Keim, D.A., 2001. On the surprising behavior of distance metrics in high dimensional space. In: Database Theory—ICDT 2001: 8th International Conference London, UK, January 4–6, 2001 Proceedings 8. Springer, Berlin Heidelberg, pp. 420–434.
Aghaei, M., Rastad, E., Shamanian, G.H., Madanipour, S., 2023. Characteristics of the gold-bearing and barren quartz veins at the Zaylik-Sarilar epithermal deposit, Ahar-Arasbaran Zone, NW Iran: evidence from mineralogy, alteration, texture and fluid inclusion. Ore Geol. Rev. 154, 105341.
Aghazadeh, M., Hou, Z., Badrzadeh, Z., Zhou, L., 2015. Temporal–spatial distribution and tectonic setting of porphyry copper deposits in Iran: constraints from zircon U–Pb and molybdenite Re–Os geochronology. Ore Geol. Rev. 70, 385–406.
Aitchison, J., 1986. The statistical analysis of compositional data. In: Monographs on Statistics and Applied Probability. Chapman & Hall Ltd., London (UK) ((Reprinted in 2003 with additional material by The Blackburn Press), London (UK). 416 p).
Alavi, M., 1991. Sedimentary and structural characteristics of the Paleo-Tethys remnants in northeastern Iran. Geol. Soc. Am. Bull. 103 (8), 983–992.
Alimohammadi, H., Chen, S.N., 2022. Performance evaluation of outlier detection techniques in production timeseries: a systematic review and meta-analysis. Expert Syst. Appl. 191, 116371.
Bellman, R., 1966. Dynamic programming. Science 153 (3731), 34–37.
Breunig, M.M., Kriegel, H.P., Ng, R.T., Sander, J., 2000, May. LOF: identifying density-based local outliers. In: Proceedings of the 2000 ACM SIGMOD International Conference on Management of Data, pp. 93–104.
Carranza, E.J.M., 2010. Mapping of anomalies in continuous and discrete fields of stream sediment geochemical landscapes. Geochemistry 10 (2), 171.
Chen, Y., Wu, W., 2017. Application of one-class support vector machine to quickly identify multivariate anomalies from geochemical exploration data. Geochem.: Explor. Environ. Anal. 17 (3), 231–238.
Chen, Y., Wu, W., 2019. Isolation forest as an alternative data-driven mineral prospectivity mapping method with a higher data-processing efficiency. Nat. Resour. Res. 28 (1), 31–46.
Chen, Y., Wu, W., Zhao, Q., 2019. A bat-optimized one-class support vector machine for mineral prospectivity mapping. Minerals 9 (5), 317.
Chen, Y., Sun, G., Zhao, Q., 2021a. Detection of multivariate geochemical anomalies associated with gold deposits by using distance anomaly factors. J. Geochem. Explor. 221, 106704.
Chen, Y., Wang, S., Zhao, Q., Sun, G., 2021b. Detection of multivariate geochemical anomalies using the bat-optimized isolation forest and bat-optimized elliptic envelope models. J. Earth Sci. 32 (2), 415–426.
Chen, Y., Zhao, Q., Lu, L., 2021c. Combining the outputs of various k-nearest neighbor anomaly detectors to form a robust ensemble model for high-dimensional geochemical anomaly detection. J. Geochem. Explor. 231, 106875.
Chen, Y., Sui, Y., Shayilan, A., 2023. Constructing a high-performance self-training model based on support vector classifiers to detect gold mineralization-related geochemical anomalies for gold exploration targeting. Ore Geol. Rev. 153, 105265.
Cooke, D.R., Hollings, P., Walshe, J.L., 2005. Giant porphyry deposits: characteristics, distribution, and tectonic controls. Econ. Geol. 100 (5), 801–818.
Dilek, Y., Imamverdiyev, N., Altunkaynak, Ş., 2010. Geochemistry and tectonics of Cenozoic volcanism in the Lesser Caucasus (Azerbaijan) and the peri-Arabian region: collision-induced mantle dynamics and its magmatic fingerprint. Int. Geol. Rev. 52 (4–6), 536–578.
Esmaeiloghli, S., Tabatabaei, S.H., Carranza, E.J.M., 2023. Infomax-based deep autoencoder network for recognition of multi-element geochemical anomalies linked to mineralization. Computers & Geosciences 175, 105341.
Fawcett, T., 2006. An introduction to ROC analysis. Pattern Recogn. Lett. 27 (8), 861–874.
Ghezelbash, R., Maghsoudi, A., 2018. Comparison of U-spatial statistics and C–A fractal models for delineating anomaly patterns of porphyry-type Cu geochemical signatures in the Varzaghan district, NW Iran. Compt. Rendus Geosci. 350 (4), 180–191.
Ghorbani, M., 2013. The economic geology of Iran. In: Mineral Deposits and Natural Resources. Springer, pp. 1–450.
Hajihosseinlou, M., Maghsoudi, A., Ghezelbash, R., 2024a. Intelligent mapping of geochemical anomalies: Adaptation of DBSCAN and mean-shift clustering approaches. J. Geochem. Explor. 258, 107393.
Hajihosseinlou, M., Maghsoudi, A., Ghezelbash, R., 2024b. A comprehensive evaluation of OPTICS, GMM and K-means clustering methodologies for geochemical anomaly detection connected with sample catchment basins. Geochemistry 84, 1–18.
Hassanpour, S., 2013. The alteration, mineralogy and geochronology (SHRIMP U–Pb and 40 Ar/39 Ar) of copper-bearing Anjerd skarn, north of the Shayvar Mountain, NW Iran. International Journal of Earth Sciences 102, 687–699.
Hodge, V., Austin, J., 2004. A survey of outlier detection methodologies. Artif. Intell. Rev. 22, 85–126.
Hyvärinen, A., 1999. The fixed-point algorithm and maximum likelihood estimation for independent component analysis. Neural. Process. Lett. 10, 1–5.
Iwamori, H., Albarède, F., 2008. Decoupled isotopic record of ridge and subduction zone processes in oceanic basalts by independent component analysis. Geochem. Geophys. Geosyst. 9 (4).
Iwamori, H., Albaréde, F., Nakamura, H., 2010. Global structure of mantle isotopic heterogeneity and its implications for mantle differentiation and convection. Earth Planet. Sci. Lett. 299 (3–4), 339–351.
Jamali, H., Dilek, Y., Daliran, F., Yaghubpur, A., Mehrabi, B., 2010. Metallogeny and tectonic evolution of the Cenozoic Ahar–Arasbaran volcanic belt, northern Iran. Int. Geol. Rev. 52 (4–6), 608–630.
Kouhestani, H., Mokhtari, M.A.A., Chang, Z., Stein, H.J., Johnson, C.A., 2018. Timing and genesis of ore formation in the Qarachilar Cu-Mo-Au deposit, Ahar-Arasbaran metallogenic zone, NW Iran: evidence from geology, fluid inclusions, O–S isotopes and Re–Os geochronology. Ore Geol. Rev. 102, 757–775.
Kriegel, H.P., Schubert, M., Zimek, A., 2008, August. Angle-based outlier detection in high-dimensional data. In: Proceedings of the 14th ACM SIGKDD International Conference on Knowledge Discovery and Data Mining, pp. 444–452.
Li, Z., Zhao, Y., Botta, N., Ionescu, C., Hu, X., 2020, November. COPOD: copula-based outlier detection. In: 2020 IEEE International Conference on Data Mining (ICDM). IEEE, pp. 1118–1123.
Liu, B., Guo, S., Wei, Y., Zhan, Z., 2014. A fast independent component analysis algorithm for geochemical anomaly detection and its application to soil geochemistry data processing. J. Appl. Math. 2014.
Liu, Y., Xia, Q., Duan, J., Dai, J., Wu, S., Zhao, Z., 2024. Geochemical anomalies of critical metals in the Eastern Kunlun Orogenic Belt, China: implications for nickel and cobalt mineral exploration. Ore Geol. Rev. 106168.

Maghsoudi, A., Yazdi, M., Mehrpartou, M., Vosoughi, M., Younesi, S., 2014. Porphyry Cu–Au mineralization in the Mirkuh Ali Mirza magmatic complex, NW Iran. J. Asian Earth Sci. 79, 932–941.
Mehrpartou, M., 1993. Geological Map of Varzaghan, Scale 1: 1,000,000. Geological survey of Iran.
Meinert, L., 1992. Skarns and skarn deposits. Geosci. Can. 19, 145–162.
Moazzen, M., Modjarrad, M., 2005. Contact metamorphism and crystal size distribution studies in the Shivar aureole, NW Iran. Geol. J. 40 (5), 499–517.
Mollai, H., Sharma, R., Pe-Piper, G., 2009. Copper mineralization around the Ahar batholith, north of Ahar (NW Iran): evidence for fluid evolution and the origin of the skarn ore deposit. Ore Geol. Rev. 35 (3–4), 401–414.
Parsa, M., Maghsoudi, A., Carranza, E.J.M., Yousefi, M., 2017. Enhancement and mapping of weak multivariate stream sediment geochemical anomalies in Ahar Area, NW Iran. Nat. Resour. Res. 26, 443–455.
Puchhammer, P., Kalubowila, C., Braus, L., Pospiech, S., Sarala, P., Filzmoser, P., 2024. A performance study of local outlier detection methods for mineral exploration with geochemical compositional data. J. Geochem. Explor. 258, 107392.
Shahrestani, S., Carranza, E.J.M., 2024. Effectiveness of LOF, iForest, and OCSVM in detecting anomalies in stream sediment geochemical data. Geochem.: Explor. Environ. Anal. 24, 1–19.
Shahrestani, S., Mokhtari, A.R., Carranza, E.J.M., Hosseini-Dinani, H., 2019. Comparison of efficiency of techniques for delineating uni-element anomalies from stream sediment geochemical landscapes. J. Geochem. Explor. 197, 184–198.
Shahrestani, S., Mokhtari, A.R., Hosseini-Dinani, H., 2018. How does sampling density affect mineralization detection in stream sediment geochemical exploration? A case study from NW of Iran. Geochemistry: Exploration, Environment, Analysis 18 (3), 196–203.
Shahrestani, S., Mokhtari, A.R., Fatehi, M., 2020. The use of unmixing technique in stream sediment geochemical exploration. J. Geochem. Explor. 208, 106339.
Shahrestani, S., Cohen, D.R., Mokhtari, A.R., 2024. A comparison of PCA and ICA in geochemical pattern recognition of soil data: the case of Cyprus. J. Geochem. Explor. 264, 107539.
Shamanian, G.H., Hattori, K., 2021. Neoproterozoic evolution of northern Gondwana recorded in detrital zircon grains from the Gheshlagh bauxite deposit, Alborz Mountains, Iran Block. Gondwana Res. 93, 184–196.
Thompson, M., Howarth, R.J., 1976. Duplicate analysis in geochemical practice. Part I. Theoretical approach and estimation of analytical reproducibility. Analyst 101 (1206), 690–698.
Wang, H., Bah, M.J., Hammad, M., 2019. Progress in outlier detection techniques: a survey. IEEE Access 7, 107964–108000.
Wang, J., Zuo, R., 2022. Model averaging for identification of geochemical anomalies linked to mineralization. Ore Geol. Rev. 146, 104955.
Yang, J., Cheng, Q., 2015. A comparative study of independent component analysis with principal component analysis in geological objects identification, part I: simulations. J. Geochem. Explor. 149, 127–135.
Yu, X., Liu, S., Ren, J., Zhang, T., Yu, X., Liu, S., Ren, J., Zhang, T., 2007. Robust fast independent component analysis applied to mineral resources prediction. In: Proceedings of the IAMG, Vol. 7, pp. 94–97.
Yu, X.C., Liu, L.W., Hu, D., Wang, Z.N., 2012. Robust ordinal independent component analysis (ROICA) applied to mineral resources prediction. J. Jilin Univ. (Earth Sci. Ed.) 42 (3), 872–880.
Zhang, T., Yu, X., Liu, L., Yu, X., Leng, H., 2007. Constrained fast independent component analysis applied to mineral resources prediction. In: Proceedings of the IAMG, Vol. 7, pp. 535–540.